Classical percolation transition in the diluted two-dimensional $S = \frac{1}{2}$ Heisenberg antiferromagnet

Anders W. Sandvik

Department of Physics, Åbo Akademi University, Porthansgatan 3, FIN-20500 Turku, Finland
(Received 24 October 2001; published 11 July 2002)

The two-dimensional antiferromagnetic $S = 1/2$ Heisenberg model with random site dilution is studied using quantum Monte Carlo simulations. Ground-state properties of the largest connected cluster on $L \times L$ lattices, with L up to 64, are calculated at the classical percolation threshold. In addition, clusters with a fixed number N_c of spins on an infinite lattice at the percolation density are studied for N_c up to 1024. The disorder averaged sublattice magnetization per spin extrapolates to the same nonzero infinite-size value for both types of clusters. Hence, the percolating clusters, which are fractal with dimensionality $d = 91/48$, have antiferromagnetic long-range order. This implies that the order-disorder transition driven by site dilution occurs exactly at the percolation threshold and that the exponents are classical. The same conclusion is reached for the bond-diluted system. The full sublattice magnetization versus site dilution curve is obtained in terms of a decomposition into a classical geometrical factor and a factor containing all the effects of quantum fluctuations. The spin stiffness is shown to obey the same scaling as the conductivity of a random resistor network.

I. INTRODUCTION

The two-dimensional (2D) Heisenberg antiferromagnet on a square lattice can be driven through a quantum phase transition[1,2] by, e.g., introducing frustrating interactions[3] or by dimerizing the lattice.[4] It has also been believed that a nontrivial (quantum) phase transition could be achieved by diluting the system, i.e., by randomly removing either sites[5–8] or bonds.[9,10] The site dilution problem is of direct relevance in the context of antiferromagnetic layered cuprates doped with nonmagnetic impurities.[11–13] Diluted Heisenberg models are also of more general interest, as systems in which the combined effects of disorder and quantum fluctuations can be studied with a variety of analytical and numerical methods. The single impurity problem has been studied extensively and is now rather well understood.[14] Systems with a finite concentration of impurities are much more difficult to treat, both analytically and numerically. The location and nature of the phase transition driven by dilution is therefore still controversial.

An early quantum Monte Carlo (QMC) study of the temperature dependence of the correlation length gave a bound $p_c > 0.2$ for the critical fraction of removed sites above which the long-range order vanishes in the 2D Heisenberg model.[5] QMC calculations in the ground state indicated $p_c \approx 0.35$.[6] Various analytical treatments have given results for p_c ranging from 0.07 to 0.30.[7,8] These estimates for the critical hole concentration are below the classical percolation threshold $p^* \approx 0.407$,[15,16] and hence the phase transition would be caused by quantum fluctuations. A critical hole density much smaller than the percolation density was also found in the bond-diluted Heisenberg model.[9,10]

An unusual type of quantum phase transition in the site diluted system was recently claimed by Kato *et al.*[17] They carried out QMC simulations of larger lattices at lower temperatures than in previous works and found evidence of the critical dilution coinciding with the classical percolation point, $p_c = p^*$. In spite of this, they argued that the transition is a nontrivial quantum phase transition, which would be a

consequence of the fractal clusters at p^* being quantum critical (i.e., with algebraically decaying spin-spin correlation function). This leads to nonclassical critical exponents, which furthermore were found to be nonuniversal, dependent on the spin S of the magnetic sites (approaching the classical values when $S \to \infty$). Although such behavior violates the standard notions of universality, it cannot be completely excluded for random systems.[18] However, in another recent study the spin correlations of the percolating 2D Heisenberg model with $S = 1/2$ were analyzed in greater detail.[19] It was confirmed that $p_c \equiv p^*$, but, in conflict with the quantum criticality scenario,[17,20,21] strong evidence was presented of a transition driven solely by percolation. The exponents should then be identical to those of classical percolation for all S.

This paper presents details of the QMC studies highlighted in Ref. 19 and introduces further evidence that the order-disorder transition in the diluted 2D Heisenberg model indeed occurs exactly at p^* and is classical. The stochastic series expansion (SSE) QMC method[22–24] is used to study the ground state of both site- and bond-diluted systems at their respective percolation points. Site-diluted systems are also studied for the whole range of hole concentrations $p < p^*$. Particular emphasis is put on the importance of carefully controlling potential sources of systematic errors in the simulations. In studies of disordered systems these issues are much more serious than for clean systems, because of the necessity to carry out a large number of relatively short simulations for different samples (in order to obtain accurate disorder averages). Procedures developed to accelerate the equilibration, and to detect possible remaining effects of insufficient equilibration and finite temperature, are discussed here and constitute an important part of the paper.

The main physics questions addressed and results obtained are summarized as follows. At the percolation point, the infinite clusters on a 2D lattice have a fractal dimensionality, $d = 91/48$.[15] An antiferromagnet at this special point could in principle be either classically critical (if there is long-range order on the fractal clusters), quantum critical (with power-law decaying spin-spin correlation function on

the clusters), or quantum disordered (with exponentially decaying correlations on the clusters). In the last of these cases, the phase transition would occur at a dilution fraction less than the percolation density, whereas it coincides with the percolation point in the other two cases. In order to determine which of the three qualitatively different ground states is realized in the percolating cluster of the standard Heisenberg model, the sublattice magnetization is calculated for the largest cluster on $L \times L$ lattices at the percolation density, with L up to 64. In addition, clusters of fixed size N_c without boundary imposed shape constraints (i.e., on an infinite 2D lattice) are studied for N_c up to 1024. The sublattice magnetization is averaged over several thousand samples and extrapolated to infinite size. The same nonzero value is obtained for both types of clusters, showing consistently that they are long-range ordered. Self-averaging is demonstrated by studying sample-to-sample distributions of the sublattice magnetization. The existence of long-range order on the percolating clusters implies that the order-disorder transition driven by dilution occurs exactly at the percolation threshold and that the critical exponents are classical. The same qualitative behavior is found for site and bond dilution, but the long-range order is substantially weaker in the bond-diluted system.

In order to reliably calculate the experimentally interesting sublattice magnetization M as a function of the site dilution fraction p for all $0 \le p < p^*$, a decomposition of $M(p)$ into a classical and a quantum-mechanical factor is used. The classical factor, which contains the singular behavior at $p = p^*$, can be easily evaluated by classical Monte Carlo simulations. The critical exponent governing its asymptotic $p \rightarrow p^*$ form is known exactly.[15] The quantum-mechanical factor is calculated using QMC simulations of the largest cluster on $L \times L$ lattices. It is only weakly dependent on the dilution. The whole $M(p)$ curve is determined to an accuracy of a few percent.

The spin stiffness is also calculated. Based on known results for the classical Heisenberg model[25] and the long-range order found here in the percolating clusters, it is argued that the stiffness should obey the same scaling as the conductivity of a random resistor network at and close to the percolation threshold. The numerical results are fully consistent with the known conductivity exponent.

The outline of the rest of the paper is the following. In Sec. II the various types of diluted Heisenberg lattices are defined, and the application of the SSE simulation algorithm to these systems is discussed. The procedures developed for controlling potential systematic errors arising from insufficient equilibration and finite temperature are also introduced here. Simulation data illustrating the convergence criteria are presented in Sec. III. In Sec. IV the sublattice magnetization of percolating clusters is studied, both for site- and bond-diluted systems. In Sec. V the full sublattice magnetization versus site-dilution curve is calculated. Results for the spin stiffness are presented in Sec. VI. The paper concludes with a summary and discussion in Sec. VII.

II. MODELS AND METHODS

The antiferromagnetic $S = 1/2$ Heisenberg model on several types of random 2D lattices will be considered. In all cases, the Hamiltonian can be written in the form

$$H = J \sum_{b=1}^{N_b} \mathbf{S}_{i(b)} \cdot \mathbf{S}_{j(b)}, \qquad (1)$$

where b is a bond index corresponding to two interacting nearest-neighbor spins $i(b), j(b)$ and N_b is the total number of bonds on the lattice. On a site-diluted lattice a fraction p of the sites are empty (holes) and the rest are occupied by spins. Bonds exist between all occupied nearest-neighbor sites. On a bond-diluted lattice all sites are occupied and nearest neighbors interact with a probability p. Note that a diluted lattice typically contains isolated (free) spins that are not interacting with any other spins. They have to be specified in addition to the list of bonds $\{i(b), j(b)\}$ in the Hamiltonian (1).

A. Diluted lattices

For lattices with $N = L \times L$ sites and periodic boundary conditions, random magnetic configurations (samples) are generated by filling each site with probability $1 - p$. The actual number of magnetic sites is hence not fixed, but the fluctuations in the density decrease as $1/L$. The percolation density $p = p^*$ is of special relevance. According to the most recent simulation,[16] $p^* = 0.407\,253\,79(13)$. Here the value $p^* = 0.407\,253\,8$ will be used. The largest cluster of connected magnetic sites is of particular interest and its properties will be studied separately from those of the full lattice. The number of spins belonging to the largest cluster is denoted by N_c. At $p = p^*$, in the limit $L \rightarrow \infty$, this cluster is fractal, with the fractal dimension d known rigorously to be $d = 91/48$.[15] For large L the average $\langle N_c \rangle \sim L^d$, and N_c is therefore typically considerably smaller than the total number of spins on the lattice. One can therefore reach larger cluster sizes in the QMC simulations by removing the spins that do not belong to the largest cluster. This will be done here in order to study the clusters for L as large as 64. An example of a diluted lattice and its largest cluster is shown in Fig. 1.

The largest cluster on a lattice at $p = p^*$ exhibits strong size fluctuations, as shown in Fig. 2. As an alternative to approaching the infinite fractal lattice as a function of L with fluctuating N_c, clusters with fixed N_c and shapes not restricted by lattice boundaries will also be studied. Such clusters are constructed starting from an infinite 2D lattice with only a single filled site. The four neighbors of this site are filled at random with probability $1 - p^*$. In the next step the neighbors of those sites that were filled are in turn filled with probability $1 - p^*$, taking into account that sites that were previously visited should not be visited again. This procedure is repeated until no new sites can be filled that are connected to the cluster, i.e., the nearest neighbors of all sites in the cluster have already been visited. If the cluster is completed before it reaches the desired size N_c, or if the size exceeds N_c, the cluster building is restarted. The process is repeated until a cluster is completed exactly at the size N_c. This method of constructing fixed-size clusters becomes very
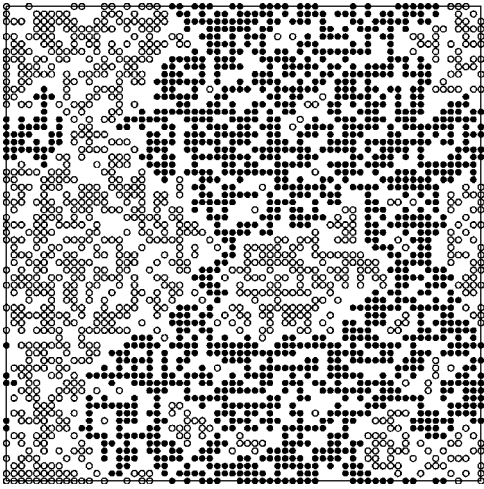
FIG. 1. A 64×64 lattice randomly diluted at $p = p^*$. The solid circles indicate magnetic sites belonging to the largest connected cluster (note that periodic boundary conditions are applied). The other magnetic sites are shown as open circles.

time consuming for large N_c, but it works well for sizes $N_c \lesssim 1024$ considered here. An example of this type of cluster is shown in Fig. 3.

In the case of bond dilution, the percolation point is exactly $p^* = 1/2$.[15] For $L \times L$ lattices this probability can be realized for any L and therefore random lattices with exactly half of the bonds removed will be considered in calculations at the percolation threshold.
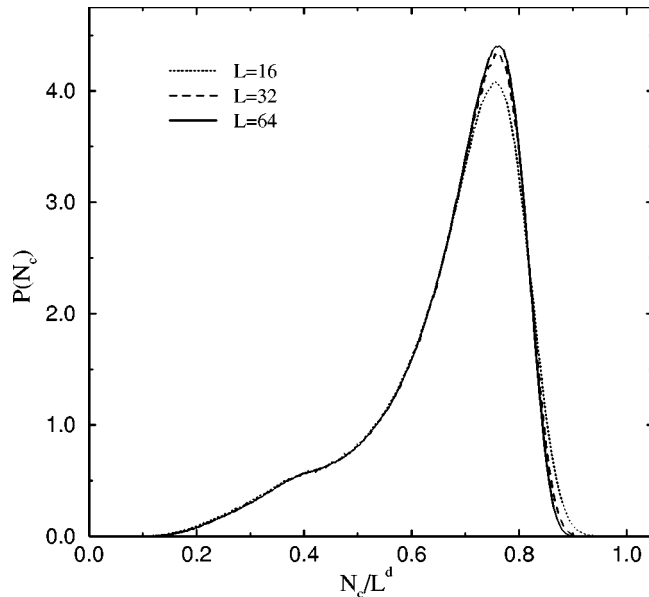
FIG. 2. Distribution of the size of the largest cluster on periodic $L \times L$ lattices for $L = 16$, 32, and 64. The probability $P(N_c)$ of cluster size N_c is plotted vs N_c / L^d, showing scaling with the fractal dimension $d = 91/48$. Note the structure at $N_c / L^d \approx 0.38$, which corresponds to lattices where instead of one dominant large cluster there are two of approximately half the size.

FIG. 3. A cluster with $N_c = 1024$ sites constructed on an infinite 2D lattice at the percolation density.

B. Quantum Monte Carlo algorithm

The SSE approach to QMC simulation of lattice models[22] has been discussed in detail in previous papers. Its application to the Heisenberg model is discussed in, e.g., Refs. 23, 24, and 26. Its effectiveness for various ordered and disordered systems has recently been documented by several groups.[27–30] Here only a very brief summary will be given, in order to facilitate the subsequent discussion of procedures developed for efficient equilibration and ground state convergence for disordered systems.

In order to apply the SSE method to the Heisenberg model, the Hamiltonian (1), with $J = 1$ hereafter, is first written as

$$H = -\sum_{b=1}^{N_b} [H_{1,b} - H_{2,b}], \qquad (2)$$

where the pair interaction has been divided into terms

$$H_{1,b} = \frac{1}{4} - S_{i(b)}^z S_{j(b)}^z, \qquad (3)$$

$$H_{2,b} = \frac{1}{2} [S_{i(b)}^+ S_{j(b)}^- + S_{i(b)}^- S_{j(b)}^+], \qquad (4)$$

which are diagonal and off diagonal, respectively, in the basis $\{|\alpha\rangle\} = \{|S_1^z, S_2^z, \ldots, S_N^z\rangle\}$ used in the simulations. A constant has been added to the diagonal part, and as a result all nonvanishing matrix elements equal $1/2$ and correspond to operations on antiparallel spins.

The SSE algorithm is based on importance sampling of the terms of the partition function $Z = \text{Tr}\{e^{-\beta H}\}$ written in a truncated Taylor expansion form,

$$Z = \sum_{\alpha} \sum_{S_M} \frac{\beta^n (M-n)!}{M!} \left\langle \alpha \left| \prod_{i=1}^{M} H_{a_i, b_i} \right| \alpha \right\rangle. \qquad (5)$$

The summation symbol S_M refers to a sequence of M operator-index pairs,

$$S_M = [a_1, b_1], [a_2, b_2], \ldots, [a_M, b_M], \tag{6}$$

where $a_i \in \{1,2\}$, $b_i \in \{1, \ldots, N_b\}$, corresponding to the operators H_{a_i, b_i} in Eqs. (3) and (4), or $[a_i, b_i] = [0,0]$, corresponding to an identity operator $H_{0,0} \equiv I$. This new operator has been introduced in order for the summation over all S_M in Eq. (5) to imply summation of the Taylor expansion of $e^{-\beta H}$ up to order M. The order of a given term corresponds to the number of non-$[0,0]$ elements in S_M, which is denoted by n in Eq. (5). It has been assumed that the lattice is bipartite. All the signs arising from the off-diagonal operators $H_{2,b}$ in Eq. (2) then cancel in the nonvanishing terms of Eq. (5) and the expansion is hence positive definite. The cutoff M can be easily adjusted so that n never reaches M during the simulation. The truncation then does not constitute an approximation, and SSE simulation results are thus exact to within statistical errors. As will be explained further below, M has to be chosen proportional to $N\beta$.

For the sampling of the terms (α, S_M) an efficient algorithm with three basic updates has been developed. The first update involves only diagonal operators. The sequence S_M is scanned from $i=1$ to M, and for each element $[a_i, b_i]$ with $a_i = 0$ or $a_i = 1$ a substitution $[0,0] \leftrightarrow [1,b_i]$ is attempted. The Metropolis acceptance probability can be easily calculated from Eq. (5), taking into account also that an update in the $\rightarrow$ direction is allowed only if the spins at the tentative bond b_i are antiparallel after operation with the previous $i-1$ operators. An accepted single-operator update changes the expansion power n in Eq. (5) by ± 1.

The second update is a more complicated cluster-type update which operates at fixed n and simultaneously changes the operator-type index of several elements $\{i\}$. The set $\{i\}$ forms an "operator loop," the size of which can be very large. For each i the substitution $[1,b_i] \leftrightarrow [2,b_i]$ can be carried out without changing the configuration weight. The whole sequence S_M can be uniquely decomposed into a number of operator loops, which can be updated independently of each other with probability 1/2. Details of this operator-loop update are discussed in Ref. 24.

Spins in the state $|\alpha\rangle$ that are not acted upon by any operator in S_M are flipped with probability 1/2. Apart from isolated spins on a diluted lattice, such free spins appear frequently only at high temperatures.

With the three updates described above—single operator (or diagonal), operator loop, and spin flip—the SSE method is completely grand canonical, i.e., all magnetization and winding number sectors are sampled. In systems with no isolated spins, the spin flip is strictly not needed, but it is still useful at high temperatures.

The simulation is started with an arbitrary state $|\alpha\rangle$ and a short index sequence containing only $[0,0]$ elements (any M will do—in the work discussed here $M = N_b/4$ was typically used). M is adjusted during the equilibration of the simulation, so that it always exceeds the maximum n reached (by, e.g., 20%), and is thereafter kept constant. A Monte Carlo step (MC step) consists of a full sweep of single-operator updates followed by construction and updates of all operator loops. After this, free spins in the state $|\alpha\rangle$ are flipped with

probability 1/2. Further details of the sampling procedures have been described in Refs. 24 and 26.

In the computer, an operator $[a,b]$ can be represented by a single four-byte integer. In addition, in the cluster update four integers are needed to store each operator element in S_M with their pointers to other elements in the list.[24] The total memory requirement is thus $20 \times M$ bytes,[31] plus a few arrays the sizes of which scale linearly with the system size N. The number of operations needed for carrying out one MC step scales as M, i.e., is proportional to $N\beta$.

Observables are typically measured after every MC step (it is often practical to do the calculations in combination with the single-operator update). Estimators for various expectation values of interest in the context of the Heisenberg model have been discussed in Ref. 23. In the present work, the most important quantity is the staggered structure factor, defined on the whole $L \times L$ lattice as (for a given disorder realization, with $S^z = 0$ on the nonmagnetic sites)

$$S(\pi, \pi) = \frac{1}{N} \left\langle \left(\sum_{i=1}^{N} (-1)^{x_i + y_i} S_i^z \right)^2 \right\rangle, \tag{7}$$

and on the largest cluster C (or the single cluster on the infinite lattice),

$$S_c(\pi, \pi) = \frac{1}{N_c} \left\langle \left(\sum_{i \in C} (-1)^{x_i + y_i} S_i^z \right)^2 \right\rangle. \tag{8}$$

Disorder averaged sublattice magnetizations are defined in terms of the structure factors according to

$$\langle m^2 \rangle = \langle 3 S(\pi, \pi)/N \rangle, \tag{9}$$

$$\langle m_c^2 \rangle = \langle 3 S_c(\pi, \pi)/N_c \rangle, \tag{10}$$

where, in the standard way,[32] the factor 3 accounts for rotational invariance in spin space. The order parameter m_c defined on a cluster will hereafter be referred to as the cluster magnetization.

The spin stiffness will also be discussed. For the nonrandom 2D Heisenberg model with periodic boundary conditions it is defined as[33]

$$\rho_s = \frac{3}{2} \frac{1}{L^2} \frac{\partial^2 E_0(\phi)}{\partial \phi^2}, \tag{11}$$

where ϕ is a twist under which the interaction on all bonds in one lattice direction is modified according to

$$\mathbf{S}_i \cdot \mathbf{S}_j \rightarrow \mathbf{S}_i \cdot R(\phi) \mathbf{S}_j, \tag{12}$$

where R is the matrix rotating the three-component spin vector $\mathbf{S}_j$ by an angle ϕ around the spin-z axis. The stiffness can be expressed in terms of the winding number of the SSE configurations. The winding number W_a, $a = x, y$, is the net number of times spin currents wrap around the system in the lattice direction a, i.e.,

$$W_a = (N_a^R - N_a^L)/L, \tag{13}$$

where N_a^R and N_a^L are the number of events in the propagation with the SSE operator sequence S_M in which spin is transported to the "left" and "right" along the a direction.

The winding numbers hence take integer values $0, \pm 1, \pm 2, \ldots$. The stiffness is given by

$$\rho_s = \frac{3}{2} \langle W_a^2 \rangle / \beta, \qquad (14)$$

which can be averaged over the two directions $a = x, y$.

For random systems the situation is complicated by the fact that the stiffness can vary locally, whereas the winding number estimator (14) is a global quantity characterizing the rigidity of the system as a whole (i.e., the energy increase due to changed boundary conditions). This global stiffness is still an important quantity, however. One can easily prove that it is equivalent to an average stiffness. In a clean system, the definition (11) can clearly be replaced by a definition where the twist (12) is only applied on a single boundary column (which has L interacting pairs),

$$\rho_s = \frac{3}{2} \frac{1}{L^2} \frac{\partial^2 E_0(\Phi)}{\partial \Phi^2}. \qquad (15)$$

The boundary twist here is related to the twist in the first definition (11) by $\Phi = L\phi$. If this definition is used for a diluted system one still obtains the same expression (14) in terms of the squared winding number, regardless of which column is taken as the boundary to which Φ is applied. This is because the spin currents wrapping around the system have to go through all L columns. The number of interacting pairs on the boundary column can depend on which of the L possible columns is used, however, and the currents are therefore distributed unequally among the bonds although the same net current passes through all columns. This reflects the local variation in the rigidity of individual bonds. The stiffness defined according to the equivalent definitions (11), (15), and (14) is hence the average over all bonds of an arbitrary column. In the case that there is no cluster wrapping around the system in either the x or y direction, the corresponding winding number is always zero and the stiffness in that direction vanishes. Recent discussions of the stiffness of disordered quantum systems can also be found in Refs. 34 and 35.

The bond energy, including the constant added in Eq. (3), is obtained in SSE simulations according to

$$E_b = -\langle H_{1,b} + H_{2,b} \rangle = -\langle n_b \rangle / \beta, \qquad (16)$$

where n_b is the number of elements $[1,b]$ and $[2,b]$ in S_M. Hence, the average expansion power $\langle n \rangle = |E|\beta$, where E is the total internal energy. One can also show that the heat capacity $C = \langle n^2 \rangle - \langle n \rangle^2 - \langle n \rangle$, and hence the width of the distribution of n is $\sim \langle n \rangle^{1/2}$ at low temperatures. This is the reason why the Taylor expansion can be truncated at $M \sim N\beta$.

C. Convergence issues

In QMC studies of random systems, disorder-averaged expectation values of the form

$$\langle\langle A \rangle\rangle = \frac{1}{N_R} \sum_{i=1}^{N_R} \langle A \rangle_i \qquad (17)$$

normally have to be estimated using only a small subset of all N_R disorder realizations. In addition, the individual expectation values $\langle A \rangle_i$ are not evaluated exactly but are associated with statistical errors. Typically $\langle A \rangle_i$ is a simple operator expectation value [such as the staggered structure factor (7) or (8)] which has an estimator that is linearly averaged over the importance sampled QMC configurations. In principle, the most efficient way to estimate the disorder average (17) would then be to generate only a single QMC configuration for each randomly selected disorder realization, so that each term contains both sources of fluctuations (sample-to-sample and QMC statistical). The final statistical error can be estimated in the standard way using data binning (in order to approach a Gaussian distribution from which the standard deviation of the average can be calculated). However, in practice this approach is not feasible since the simulations have to be properly equilibrated for each disorder realization before the QMC configurations can be used for averages. If a large number of MC steps are needed for equilibration it would clearly not be optimal to make use of only a single configuration. An accurate estimation of the optimum number of configurations would require detailed knowledge of equilibration times, autocorrelation times, and the statistical distributions of the estimators. In practice, it is rarely worthwhile to investigate these in detail (it would require an effort rivaling that of the actual simulations). In any case, the simulations should be relatively short so that many disorder realizations can be studied. Furthermore, the simulations should not be dominated by equilibration. The number of MC steps used for sampling expectation values should therefore be at least of the same order as the number of steps used for equilibration.

Another important issue is temperature. In order to study ground-state properties with the SSE method, a sufficiently high inverse temperature β must be used. In diluted systems, especially close to the percolation point, different parts of a large cluster may be connected only weakly, through essentially one-dimensional narrow paths (several examples of which can be seen in Figs. 1 and 3). Such "weak links" can lead to correlations that develop only at very low temperatures. One can therefore expect that in order to reach the ground state much higher β values have to be used than for undepleted 2D systems.

Remaining temperature effects and insufficient equilibration are two potential sources of systematic errors in the simulations, and these have to be controlled very carefully. The following scheme has been developed in order to check for both equilibration and temperature effects. For each disorder realization, simulations are carried out at inverse temperatures $\beta_n = 2^n$, $n = 0, 1, \ldots, n_{\max}$. Starting with $n = 0$ ($\beta = 1$), a number N_e of MC steps are first carried out for equilibration. Expectation values are sampled during the following $N_m = 2N_e$ steps. At the same temperature, N_e additional steps are carried out during which no expectation values are sampled, again followed by N_m sampling steps. The second segment of $N_e + N_m$ steps is a direct continuation of the first one, so that the effective number of equilibration steps for the second sampling segment is four times that for the first one. A disagreement between the results of the two
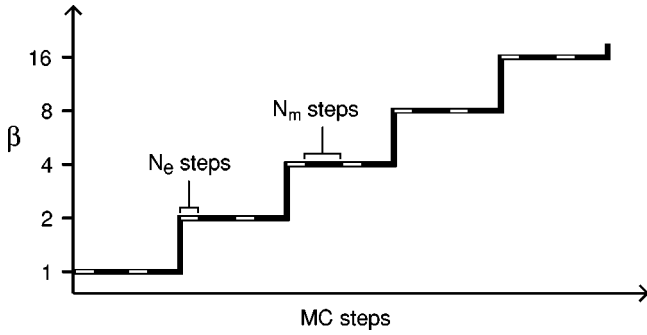
FIG. 4. Illustration of the β-doubling scheme used for equilibration and convergence to the ground state. The horizontal line segments represent MC steps carried out at the corresponding inverse temperatures $\beta = 2^n$. No data are collected during the N_e steps corresponding to the unfilled segments. Averages over the two solid segments of length N_m are stored separately for each β.

sampling segments then implies that the simulation at the level of the first segment is not sufficiently equilibrated, and the second segment may also be affected. If the results agree, one can conclude that at least the second segment should have equilibration errors that are smaller than the statistical errors (although this should also be verified by comparing simulations with different N_m, which will be done below). Since the fluctuations of the results of short simulations are large, the agreement between the two segments can of course be checked only in averages over large numbers of simulations of different disorder realizations.

The β-doubling scheme is illustrated in Fig. 4. Note that simulations at subsequently lower temperatures can be started using the last SSE configuration generated at the previous temperature. An equilibrated configuration at β will have an SSE sequence length M approximately twice that in the previous run at $\beta/2$. Therefore, in order to further accelerate the equilibration at low temperatures, the starting sequence used is the previous S_M doubled, i.e.,

$$S_{2M} = [a_1, b_1], \ldots, [a_M, b_M][a_M, b_M], \ldots, [a_1, b_1]. \quad (18)$$

Especially at low temperatures, where the system is almost converged to the ground state, the doubled SSE configuration should be very nearly distributed according to the equilibrium distribution at the new β. With the reversed order of the second set of M operators in Eq. (18), the initial S_{2M} always has zero winding number, which can be expected[36] to be a slightly better starting point than the alternative one with twice the winding number (in practice, the difference in performance is minor).

Expectation values calculated for all $n_{max} + 1$ values of β are stored on disk, so that the convergence to the ground state can be checked. Ideally, the number of β doublings should be large enough that there are no statistically significant differences between the results for $\beta_{max} = 2^{n_{max}}$ and $\beta = 2^{n_{max}-1}$. Since the asymptotic convergence is exponential, the results at β_{max} should then have no detectable temperature effects at the level of the statistical errors.
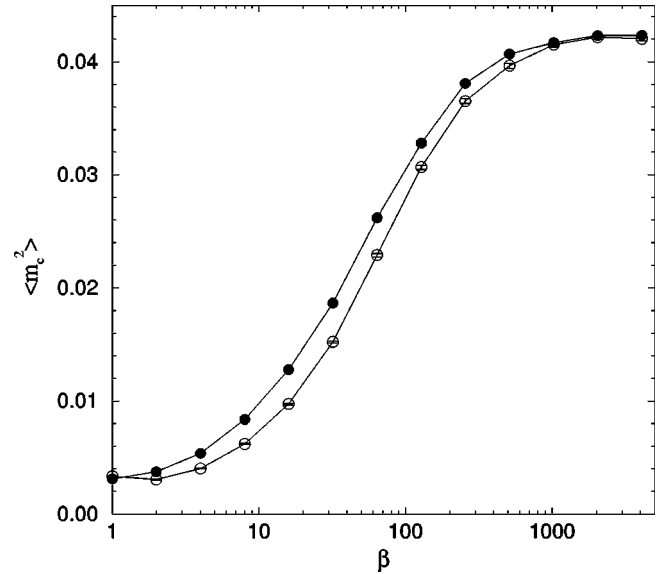
FIG. 5. Test results for the convergence of the sublattice magnetization of the largest cluster on 32×32 lattices at p^*. The number of MC steps for averaging data for each point was $N_m = 2$. The open and solid circles correspond to the first and second data collection segment, respectively. The results are averages over 10^4 disorder realizations.

III. CONVERGENCE TESTS

In this section, test results for equilibration and ground-state convergence according to the β-doubling procedures described in the preceding section are presented. Dilution fractions close to the percolation point can be expected to be the worst with respect to slow β convergence. This is because for $p < p^*$ the largest clusters are two dimensional and more compact than at p^* (i.e., they have less ''weak links''), and for $p > p^*$ the cluster size does not diverge with L. Site-diluted systems exactly at the percolation point are considered here.

A. Equilibration

The equilibration of the simulations will first be illustrated by results for $L = 32$ systems obtained with different N_e and $N_m = 2N_e$. Figure 5 shows results for the disorder averaged cluster magnetization when the segments are very short, $N_e = 1$ and $N_m = 2$. At the highest temperature, $\beta = 1$, the two segments give results that agree within statistical errors, but as the temperature is lowered the results begin to differ considerably. At still lower temperatures the results again converge and become statistically indistinguishable at $\beta = 1024$ in this case. The good agreement here can be explained by the fact that low-temperature simulations in the β-doubling procedure start from configurations that already have a rather long history at higher temperatures, which in combination with the trick of doubling the SSE operator sequence produces almost equilibrated initial configurations when the system is nearly in its ground state.

Figure 6 shows how results at an intermediate and low temperature depend on the number of MC steps in the data collection segments. At $\beta = 32$, the first data segment con-
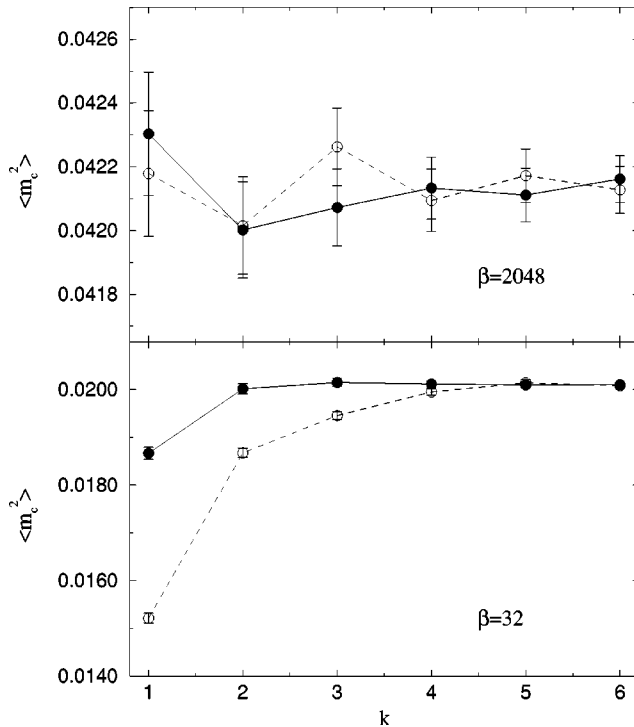
FIG. 6. Dependence of the calculated cluster magnetization on the number of MC steps in the data collection segments, $N_m = 2^k$, at two different inverse temperatures (results for $L = 32$ lattices at p^*, averaged over 10^4 samples). The open and solid circles correspond to the first and second data collection segment, respectively.

FIG. 7. Distribution of the cluster magnetization of 32×32 lattices at p^* for different lengths of the data collection segments. The inverse temperature $\beta = 4096$, and 10^4 disorder realizations were used for each N_m.

verges after $N_m \gtrsim 16$, whereas the second segment appears to be converged already for $N_m = 4$. At $\beta = 2048$, the results for the two segments agree statistically for all N_m, and the averages show no discernible dependence on N_m. Hence, an agreement between the two segments indeed appears to be a good indication of sufficient equilibration. Since the convergence is the slowest at intermediate temperatures, a very safe conservative check of low-temperature equilibration should be that the two segments agree at all temperatures. For the final result, the segments can then be averaged in order to improve the statistics. However, this typically leads only to a modest reduction of the error bars (i.e., significantly less than the reduction by $\sqrt{2}$ expected for independent data) since the statistical errors are dominated by fluctuations between the disorder realizations. The fact that sample-to-sample fluctuations dominate can also be seen clearly in Fig. 6, where the error bars decrease much slower than by $\sqrt{2}$ for successively higher k.

The results presented here indicate that even extremely short simulations give results void of nonequilibration effects at low temperatures. However, longer runs were used to produce some of the data presented in this paper. The main reason for this is that although unbiased disorder averages of the form (17) can be obtained with short simulations, large statistical errors in the individual expectation values can be problematic when considering nonlinear functions of the expectation values (such as their typical values) or their complete statistical distributions. One then has to demand that the statistical errors of the individual expectation values are

much smaller than the width of the distribution of the exact expectation values. An example of how statistical errors can distort distributions is shown in Fig. 7, where histograms of the cluster magnetization are compared for six different simulation lengths. Both the data collection segments were used for calculating the individual expectation values, i.e., the number of measurements for each realization is $2N_m$. The histograms become significantly narrower as the number of MC steps is increased. The distribution is not completely converged even for the longest simulation considered here ($N_m = 64$), but the relatively small differences between $N_m = 32$ and 64 suggest that the $N_m = 64$ result is close to the exact distribution. Note that the first moment of the distribution, i.e., the linear disorder average (17), is the same within statistical errors for all N_m (which was demonstrated at $\beta = 2048$ in Fig. 6).

In the calculations discussed in the following sections, N_m between 100 and 250 was used to ensure that reliable distributions could be obtained at the percolation point. For $p < p^*$, where the full distributions are not as important, $N_m = 50$ was typically used. Since effects of insufficient equilibration are undetectable even in much shorter simulations the results should definitely be void of any bias of this nature.

B. Ground-state convergence

Already the results shown in Fig. 5 demonstrate that very low temperatures are required in order to converge the sublattice magnetization to its ground-state value. For $L = 32$, a β value higher than 2000 is needed to eliminate temperature effects within the statistical errors. In order to more accurately study remaining effects at low temperatures it is useful to calculate ratios $\langle m_c^2(\beta_i) \rangle / \langle m_c^2(\beta_j) \rangle$ of the squared cluster
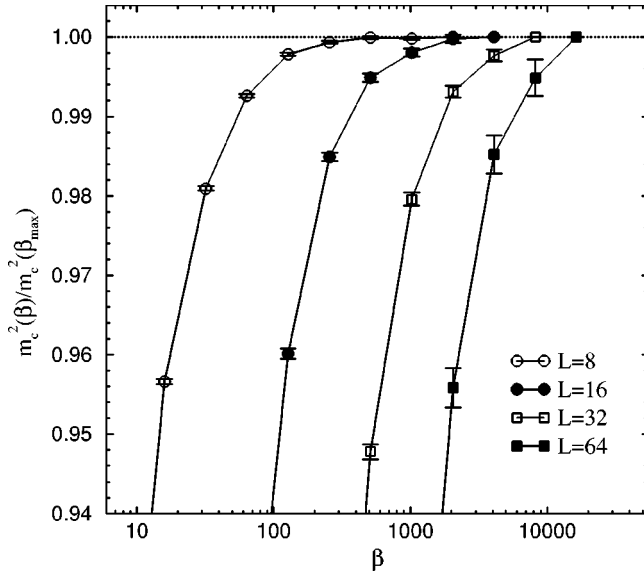
FIG. 8. Cluster magnetization ratios vs inverse temperature for $L \times L$ lattices. The number of samples used for averaging the results was 88 000, 21 000, 9000, and 2500, for $L = 8$, 16, 32, and 64, respectively.

FIG. 9. Magnetization ratios vs inverse temperature for fixed-N_c clusters. The number of samples was 43 000, 15 000, 10 000, 3000, and 1100, for $N_c = 64,128,256,512$, and 1024, respectively.

magnetization at different temperatures. The relative statistical errors are smaller in the ratios than in the absolute values, since the sample-to-sample fluctuations cancel when the same realizations are used at all temperatures. Figure 8 shows results for systems with $L = 8$, 16, 32 and 64, which were simulated with β up to $\beta_{max} = 256 \times L$. The ratios, with the data at the respective β_{max} in the denominator, were analyzed using the bootstrap method[37] in order to obtain accurate estimates of the error bars. For $L = 8$ and $L = 16$, the results at β_{max} and $\beta_{max}/2$ do not differ within statistical errors and hence the result at β_{max} should not have any temperature effects left at this precision level. The $L = 32$ and 64 results are not completely converged to the ground state, however. The exponential low-temperature convergence seen for all the system sizes indicates that the remaining temperature effects at β_{max} should only lead to an error that is smaller than the difference between the ratios at β_{max} and $\beta_{max}/2$. Hence, the underestimation of the sublattice magnetization should be less than 0.2% for $L = 32$ and less than 0.5% for $L = 64$. These upper bounds for the systematic errors are of the same magnitude as the respective statistical errors in $\langle m_c^2 \rangle$ (which unlike the ratios also include contributions from sample-to-sample fluctuations). The remaining small temperature effects should therefore not substantially affect the finite-size scaling of the sublattice magnetization (to be discussed in the following section).

Figure 9 shows magnetization ratios for fixed-N_c clusters, with $\beta_{max} = 32 \times N_c$. In this case there are small but detectable differences between the results at β_{max} and $\beta_{max}/2$ for all system sizes, except for $N_c = 1024$ where the statistical error is larger than the difference. Again, the maximum relative systematic errors remaining at β_{max} are similar in magnitude to the statistical fluctuations in $\langle m_c^2 \rangle$ and can only have very minor effects on the finite-size scaling.
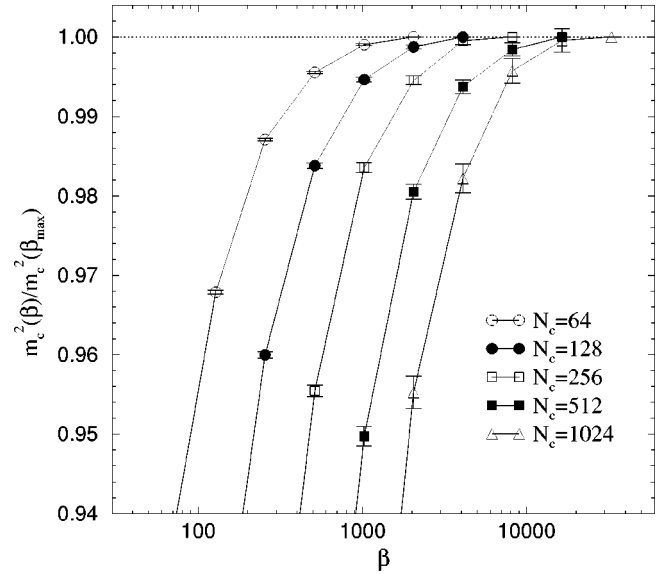
The β needed for ground-state convergence decreases rapidly away from the percolation point, and therefore the $p < p^*$ results for $L \times L$ lattices discussed in Secs. V and VI are completely converged even for $L = 64$.

IV. LONG-RANGE ORDER IN PERCOLATING CLUSTERS

In this section, the ground-state sublattice magnetization of the percolating cluster is investigated in detail. If it remains finite in the thermodynamic limit, the order-disorder transition driven by dilution must necessarily occur exactly at the classical percolation density. To see this, consider the sublattice magnetization (9) of the diluted $L \times L$ lattice. Its disorder average can be written as a sum of contributions from all the clusters k on the lattices as

$$\langle m^2 \rangle = \frac{1}{N^2} \left\langle \sum_k N_k^2 m_k^2 \right\rangle. \tag{19}$$

In the thermodynamic limit, only infinite clusters contribute to this sum, and therefore one only needs to consider the behavior of the cluster magnetizations m_k^2 for large clusters. If there is long-range order, it is natural to assume that the sublattice magnetization is self-averaging (a fact that will also be demonstrated explicitly below). The individual m_k^2 values can then be replaced by the infinite-size extrapolated average for the largest cluster, i.e., $\langle m_c^2 \rangle$, which gives

$$\langle m^2 \rangle = \frac{\langle m_c^2 \rangle}{N^2} \left\langle \sum_k N_k^2 \right\rangle \quad (L \to \infty). \tag{20}$$

This expression is identical to the order parameter of a classical diluted system, up to the factor $\langle m_c^2 \rangle$ which is reduced by quantum fluctuations from its classical value 1/4 (for an Ising model with $S_i^z = \pm 1/2$). If $\langle m_c^2 \rangle$ remains finite at $p = p^*$ [which is the condition for Eq. (20) to remain valid for

all $p \lesssim p^*$] the only singular behavior is in the classical expectation value and hence the critical behavior is that of classical percolation.

In general, Eq. (20) holds for any dilution fraction $p < p_c$, where p_c in principle may be less than p^*. The cluster magnetization $\langle m_c^2 \rangle^{1/2}$ will here be determined at percolation, where the infinite clusters are fractal. Dilutions less than the percolation density, where the infinite clusters are two dimensional, will be studied in the following section.

A. Sublattice magnetization in site-diluted systems

At the percolation point, the average number of spins in the largest cluster on a diluted $L \times L$ lattice scales asymptotically as $\langle N_c \rangle \sim L^d$, with d the fractal dimension $91/48$.[15] As can be seen in Fig. 2, the full distribution of the size of the largest cluster also scales as L^d, i.e., the distribution width also diverges as $L \to \infty$. This is in sharp contrast to the situation below the percolation threshold where the size distribution approaches a δ function at a size $\sim L^2$. Note, however, that the scaled distribution at p^* has sharp cutoffs both at the lower and upper edge, meaning that also the smallest and largest clusters grow as L^d. Hence, finite-size scaling of $\langle m_c^2 \rangle$ calculated on such fluctuating-N_c clusters as a function of L is a well defined procedure for extracting the sublattice magnetization of the infinite fractal cluster. Nevertheless, the alternative way of approaching the thermodynamic limit with fixed-N_c clusters on the infinite lattice is also considered here. An agreement between the two calculations will provide additional support to the argument[19] that the percolating cluster is ordered.

In the pure 2D Heisenberg model the leading size correction[38] to m^2 is $\sim N^{-1/2}$, which can be seen clearly in numerical data.[32,23] In analogy with this, as a scaling hypothesis at percolation, the following leading size corrections are tested here for the largest cluster on $L \times L$ lattices and fixed-N_c clusters, respectively:

$$\langle m_c^2 \rangle_L = \langle m_c^2 \rangle_\infty + aL^{-d/2}, \tag{21}$$

$$\langle m_c^2 \rangle_{N_c} = \langle m_c^2 \rangle_\infty + bN_c^{-1/2}. \tag{22}$$

Figure 10 shows results for L up to 64 and N_c up to 1024. The data are fully consistent with the scaling ansatz, although in order to fit all the points a polynomial cubic in $L^{-d/2}$ has to be used in both cases (a cubic polynomial is needed also to fit high-accuracy data for the clean 2D Heisenberg model[23]). The infinite-size extrapolated values for $\langle m_c^2 \rangle$ from the two fits agree very well (within statistical errors). The sublattice magnetization is in fact quite large, $\langle m_c \rangle = 0.150(2)$, which is almost precisely half of the value $m = 0.307$ for the clean 2D system.[32,23]

It should be stressed that it is not critical whether or not the scaling ansatz assumed here to carry out the extrapolation of the sublattice magnetization is strictly correct or not. Unless the behavior would change dramatically for even larger systems, a slightly different finite-size correction would not significantly affect the extrapolated $\langle m_c^2 \rangle$. One could of course argue that a crossover to a qualitatively different be-
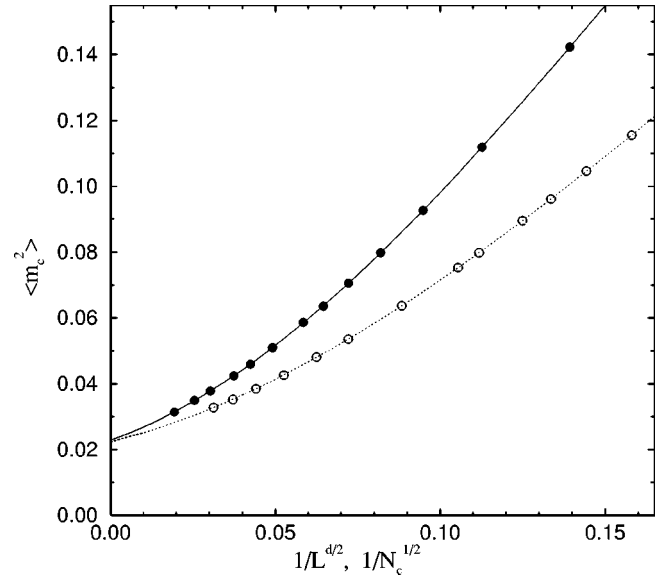
FIG. 10. Finite-size scaling of the disorder averaged squared cluster magnetization. The results for the largest cluster on $L \times L$ lattices (solid circles) are plotted vs $L^{-d/2}$ and those for fixed-N_c clusters (open circles) vs $N_c^{-1/2}$. Statistical errors are much smaller than the symbols. The curves are cubic polynomial fits.

havior cannot be excluded, as indeed has been done.[20] No plausible physical reason for such a crossover has been presented, however. With two different boundary conditions for the clusters giving the same result for the infinite-size extrapolated sublattice magnetization, the most natural scenario must be that the percolating cluster is ordered.

In a disordered system the order parameter is not constant over the whole system, but depends locally on the structure of the lattice. One would, however, expect self-averaging, i.e., the sublattice magnetization averaged over different regions of an infinite cluster should be the same when the size of the regions is sufficiently large. In finite systems, self-averaging can be seen in the statistical distributions of the individual cluster magnetizations. Figure 11 shows results at the percolation point for several $L \times L$ and fixed-N_c systems. As discussed in Sec. III, the histograms can be expected to be slightly broadened by the statistical fluctuations in the SSE results for the individual m_c^2 values. Such effects should, however, be minor when the simulations are as long as those used for the data shown here ($N_m = 100$ for the $L \times L$ lattices and 250 for the fixed-N_c clusters). The widths of both types of distributions decrease with increasing system size, which is consistent with vanishing fluctuations in the thermodynamic limit. It can also be noted that the distributions become more symmetric for larger systems—the weak tails visible at the high end of the distributions for small clusters vanish as the system grows. The behavior is hence fully consistent with the δ-function distribution expected for a self-averaging quantity in the thermodynamic limit.

It is also interesting to study how the cluster magnetization depends on the shape of the cluster. A compact cluster is likely to have a stronger order than one which has many narrow paths. A natural length scale characterizing the overall density of the unconstrained fixed-N_c clusters is the radius of gyration,
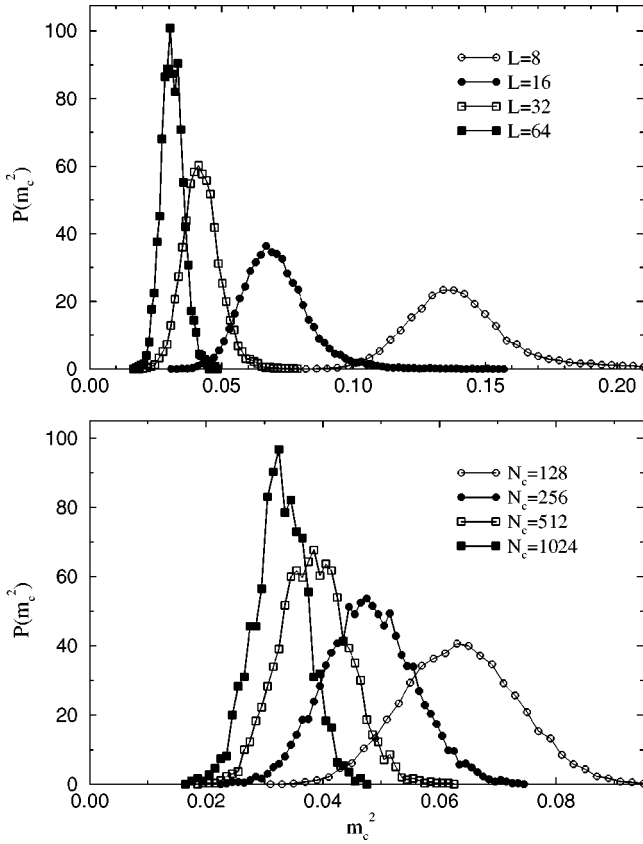
FIG. 11. Distribution of the cluster magnetization of $L \times L$ lattices (top panel) and fixed-N_c clusters on the infinite lattice (bottom panel).

$$R = \left(\frac{1}{2N_c^2} \sum_{i=1}^{N_c} \sum_{j=1}^{N_c} (x_i - x_j)^2 + (y_i - y_j)^2 \right)^{1/2}, \quad (23)$$

where x_i, y_i are the (integer) coordinates of the magnetic sites. Figure 12 shows scatter plots of the cluster magnetization versus R for two cluster sizes. For $N_c = 128$, one can see that the most compact clusters, i.e., those with the smallest R, indeed have the largest magnetizations. After an initial rapid decrease with R for the smallest R, the average magnetization only decreases slowly with increasing R, however. The $N_c = 1024$ clusters show a similar behavior. There are of course in principle clusters with very large R that should have much smaller magnetizations, but these clusters lack statistical significance. The weak R dependence for the statistically significant clusters is another manifestation of a strongly self-averaging sublattice magnetization.

B. Sublattice magnetization in bond-diluted systems

For the bond-diluted system only simulations of $L \times L$ lattices were carried out. Figure 13 shows the results for the cluster magnetization at the bond percolation point, $P^* = 1/2$, plotted in the same way as for the site-diluted systems in Fig. 10. Also in this case the scaling to a finite sublattice magnetization is evident, but the value of the order parameter is smaller than in the site-diluted system; $\langle m_c \rangle = 0.088(2)$. The difference can be explained by the different
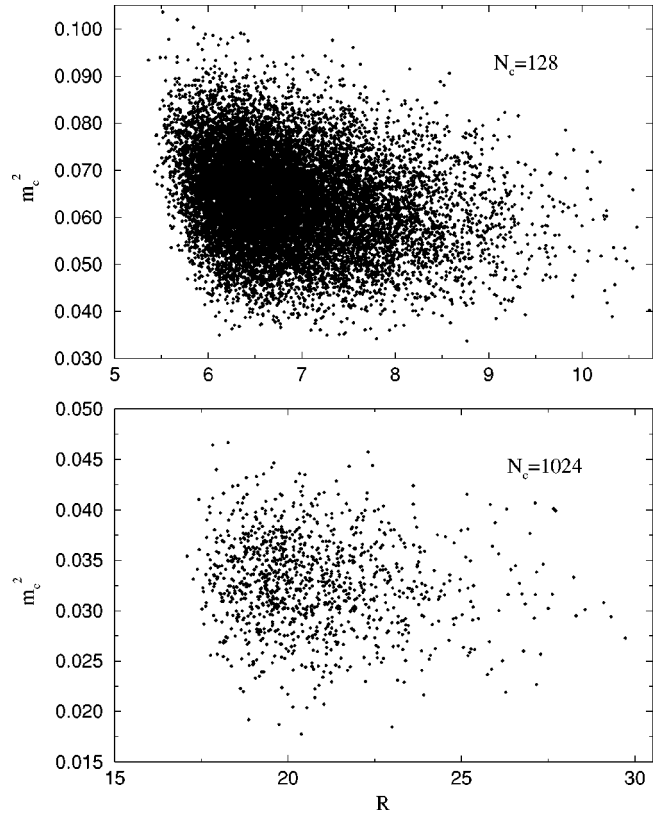
FIG. 12. Individual squared magnetizations vs the radius of gyration for clusters on the infinite lattice.

local structures of the two types of lattices. Although the fractal dimension d of the cluster is the same for site and bond percolation,[39] the average number of bonds per spin is smaller in the bond-diluted case—1.121 vs 1.259. This leads to stronger quantum fluctuations in the bond-diluted system. The infinite-size energy per bond (which reflects the ten-
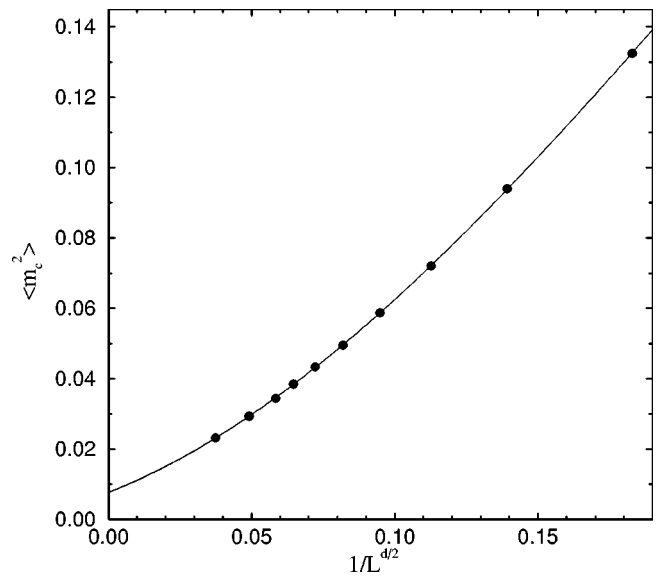
FIG. 13. Finite-size scaling of the disorder averaged squared cluster magnetization of the bond-diluted system at the percolation density. The curve is a cubic polynomial fit.
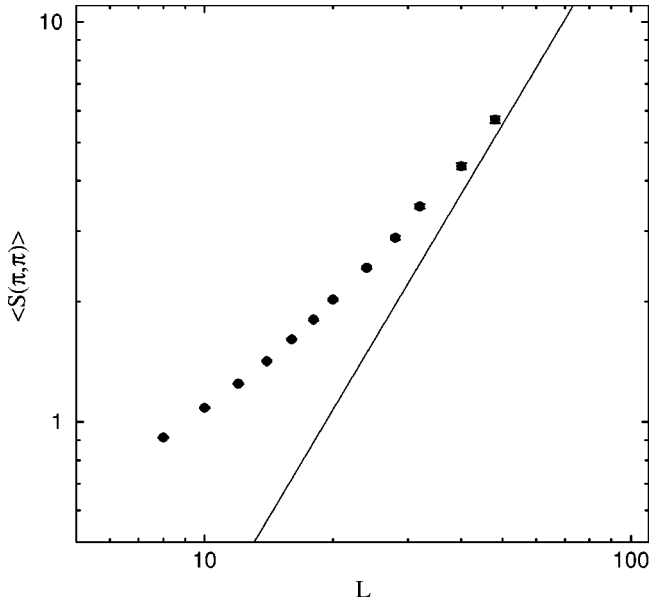
FIG. 14. Finite-size scaling of the disorder averaged staggered structure factor of the full site diluted $L \times L$ lattice. The line has slope 43/24, expected for classical percolation.

dency to nearest-neighbor singlet formation) is $-0.3890(1)$ and $-0.4068(2)$ for site and bond dilution, respectively.

It can also be noted that for a given L the average largest cluster on the bond-diluted lattice is $\approx 45\%$ larger than on the site-diluted lattice. The stronger quantum fluctuations and the larger cluster sizes imply that for given L a lower temperature has to be used to converge the bond-diluted system to the ground state. For the largest size studied in this case, $L = 32$, an inverse temperature $\beta = 32\,768$ was used.

C. Scaling of the full staggered structure factor

The previous claims of quantum criticality at the percolation point[17,21] were primarily based on a finite-size scaling analysis of the staggered structure factor. A log-log plot of $S(\pi,\pi)$ calculated using SSE simulations including all the spins of diluted $L \times L$ lattices is shown in Fig. 14. The numerical values agree well with those of Ref. 17. One can, however, expect a barely discernible finite-T reduction in the previous $L = 48$ results because the temperature used ($\beta = 1000$) was not sufficiently low for complete converge to the ground state (see Fig. 8 and a related discussion in Ref. 19).

The scaling seen in Fig. 14 is different from the expected classical percolation behavior. Given the results presented above for the scaling of the cluster magnetization, the deviation from classical behavior for this range of system sizes is not surprising, however. Classically, the finite-size scaling of $S(\pi,\pi)$ is solely the result of the divergence of the size of the connected clusters with L. In the quantum-mechanical case, there is also a factor, the sublattice magnetization of the cluster, multiplying each cluster size, i.e.,

$$\langle S(\pi,\pi) \rangle = \frac{1}{N} \left\langle \sum_k N_k^2 m_k^2 \right\rangle. \tag{24}$$

The size dependence of the average m_k^2 was shown in Fig. 10. From these results it is clear that there is an effect that partially compensates for the growth of the cluster sizes N_k in Eq. (24), namely, m_k^2 decreases with increasing cluster size. Hence, for systems where the relative size corrections to the cluster magnetization are still significant, as is the case for all sizes that can currently be reached in numerical simulations, the growth of $S(\pi,\pi)$ with L will be slower than for a classical system. This explains the slow convergence towards the classical behavior that can be seen in Fig. 14. It can be noted that the largest cluster completely dominates the staggered structure factor and the curve shown in Fig. 14 changes only very little if only the largest cluster is included, i.e., $S_c(\pi,\pi) \approx S(\pi,\pi)$.[40]

V. DILUTION DEPENDENCE OF THE SUBLATTICE MAGNETIZATION

The doping dependence of the sublattice magnetization of antiferromagnetic cuprates can be measured experimentally using nuclear quadrupole resonance, μ^+ spin resonance, and neutron scattering.[11,13] Results for the Heisenberg model were recently obtained using an improved spin-wave theory which, however, breaks down close to the percolation threshold (the critical point is unphysical, located at a hole concentration *higher* than the percolation density).[12,41] Previous QMC calculations of the doping dependence were based on Eq. (9).[17] Use of this formula becomes very difficult close to the percolation threshold, however, since the smallness of the sublattice magnetization there is associated with a slow convergence to the asymptotic regime in which finite-size scaling is reliable. Here a different approach will be taken, based on the fact that the sublattice magnetization can be decomposed into classical and quantum-mechanical factors, which can be evaluated separately. This decomposition was already discussed in Sec. IV and was written as Eq. (20). Here the notation $M = \langle m^2 \rangle^{1/2}$ will be used for the disorder averaged sublattice magnetization. Equation (20) can then be written as

$$M(p) = M_{qm}(p) M_{cl}(p) \quad (L \to \infty), \tag{25}$$

where M_{qm} is the quantum-mechanical factor

$$M_{qm} = \sqrt{\langle m_c^2 \rangle}, \tag{26}$$

and M_{cl} is the classical (geometrical) factor

$$M_{cl} = \frac{1}{N} \left\langle \sum_k N_k^2 \right\rangle^{1/2}. \tag{27}$$

In the ordered regime, $0 \leq p < p^*$, only the largest cluster contributes to this sum in the thermodynamic limit. The classical factor can therefore also be obtained as

$$M_{cl} = \langle N_c \rangle / N. \tag{28}$$

Figure 15 shows the size convergence using the two definitions of the classical factor when the dilution fraction $p = p^* - 0.005$. The single-cluster average (28) clearly converges faster. It is apparent that a reliable extraction of the
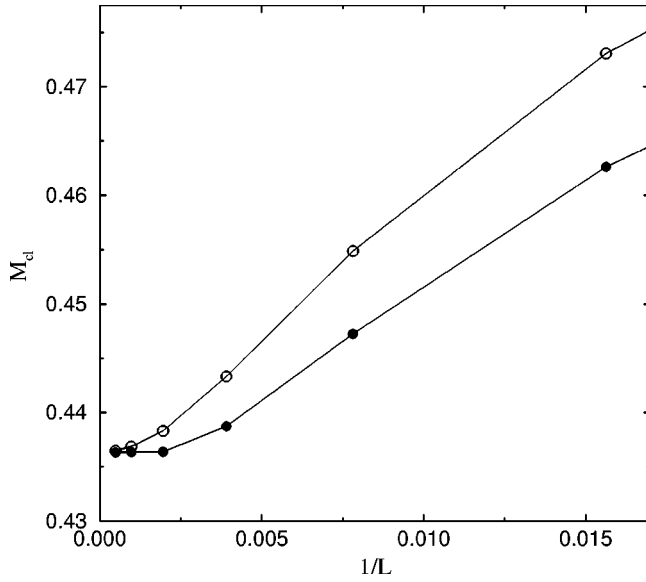
FIG. 15. Size dependence of the classical magnetization for systems diluted at one half percent less than the percolation density ($p = p^* - 0.005$). The open circles correspond to the full cluster sum, Eq. (27). The solid circles are from the average including only the largest cluster, Eq. (28).

quantum-mechanical sublattice magnetization M using the structure factor formula (9) would be impossible in this case, since not even the classical magnetization is in the asymptotic scaling regime for the range of system sizes where QMC simulations can be carried out ($L \lesssim 100$). The quantum-mechanical M can be expected to have an even worse scaling behavior, due to effects similar to those found for the staggered structure factor in Sec. IV C. The quantum-mechanical factor M_{qm} can be calculated based on much smaller system sizes, however. It was evaluated in the extreme case $p = p^*$ in Sec. IV, and even there it is as large as 50% of the value in the other extreme, i.e., the nondiluted system ($p = 0$). Hence, M_{qm} is only weakly dependent on the dilution fraction, and most of the p dependence of M, including the singular behavior at p^*, is in the classical factor M_{cl}.

The classical magnetization is known to vanish at the percolation threshold with the exponent 5/36,[15] i.e.,

$$M_{cl}(p \to p^*) = A_{cl}(p^* - p)^{5/36}. \tag{29}$$

In the weak dilution limit, one can easily obtain the result $M_{cl} = 1 - p$. Numerical values for $0 < p \lesssim p^* - 0.002$ were obtained here by simulations of lattice sizes as large as $L = 4096$, using the single-cluster estimator (28). In the example illustrated in Fig. 15, the results for the three largest sizes are 0.43 640(4), 0.43 636(3), and 0.43 634(2) (for $L = 512$, 1024, and 2048, respectively) and the $L = 2048$ result (which is based on 3×10^5 samples) can hence be taken as the infinite-size value of $M_{cl}(p^* - 0.005)$. Closer to the percolation threshold $L = 4096$ lattices were used. Figure 16 shows results for the whole dilution range. The linear small-p form describes the data well for p up to ≈ 0.2. The asymptotic form (29) is well reproduced for $p^* - p \lesssim 0.02$, with the constant $A_{cl} \approx 0.91$. In order to have an analytic
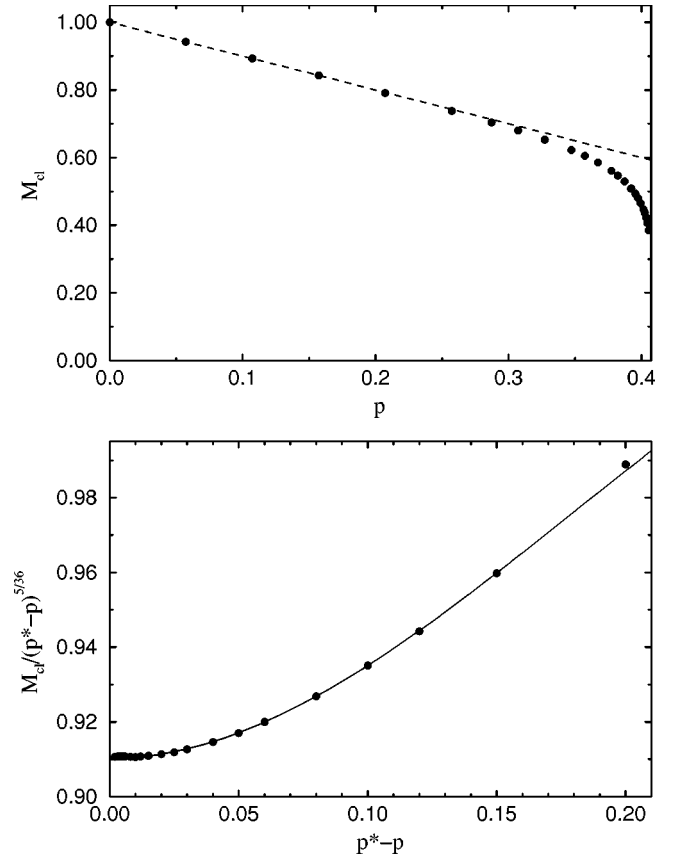
FIG. 16. Upper panel, classical magnetization vs dilution. The dashed line shows the small-p form $M_{cl} = 1 - p$. Lower panel, the magnetization divided by $(p^* - p)^{5/36}$ plotted vs $p^* - p$. The curve is a polynomial fit, with parameters given in Eq. (31).

expression describing M_{cl} in a wider region around p^*, higher-order terms can be added to A_{cl}. The following forms will be used in combination with fits to the quantum-mechanical factor in order to obtain expressions for M both close to $p = 0$ and $p = p^*$,

$$M_{cl}(p \lesssim 0.2) = 1 - p, \tag{30}$$

$$M_{cl}(p^* - p \lesssim 0.2) = [0.9102 + 3.053(p^* - p)^2$$
$$- 5.642(p^* - p)^3](p^* - p)^{5/36}. \tag{31}$$

Note that it is not claimed here that the higher-order terms in the form (31) are the correct subleading terms of the critical percolation behavior—the purpose is just to have an expression that describes the data well in practice, within the stated region.

The quantum-mechanical factor can be calculated in the same way as was already explained in the case of $p = p^*$ in Sec. IV, i.e., using the SSE method for the largest cluster of connected magnetic sites on $L \times L$ lattices. Here L up to 64 was used for dilution fractions $p = p^* - \delta$, with $\delta = 0.05$, 0.10, ..., 0.35, and 0.38. SSE simulations at $p = 0$ were previously carried out for L up to 16,[23] and were here extended up to $L = 64$. Since the ground-state convergence
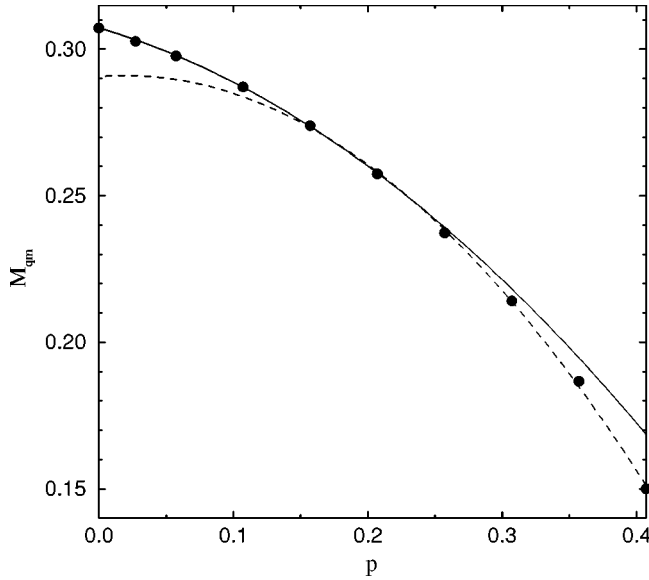
FIG. 17. The quantum-mechanical factor (cluster magnetization) vs dilution. The curves are quadratic fits (solid for small p and dashed for small p^*-p) with parameters given in Eqs. (32) and (33), respectively.

FIG. 18. Sublattice magnetization vs site dilution (solid circles). The curves are parametrized forms discussed in the text. The inset shows the behavior close to the percolation threshold on a more detailed scale.

occurs at lower β as δ is increased, the simulations are faster than at p^* and a larger number of samples could therefore be studied. The number of samples was $>10^4$ for $L=64$ and up to 10^6 for smaller lattices. The results were extrapolated to infinite size using a leading correction $\sim 1/L$ (as in the case of the clean 2D system[32]). The resulting $M_{qm}(p)$ is shown in Fig. 17, along with two quadratic fits that describe the data very well over quite wide ranges of p. The fitted forms are

$$M_{qm}(p \lesssim 0.25) = 0.3072 - 0.134p - 0.51p^2, \quad (32)$$

$$M_{qm}(p^*-p \lesssim 0.25) = 0.151 + 0.721(p^*-p) - 0.93(p^*-p)^2. \quad (33)$$

The final result for the sublattice magnetization of the site-diluted Heisenberg model is shown in Fig. 18. The solid circles were obtained by interpolating the numerical results for M_{cl} and M_{qm} and multiplying them according to Eq. (25). Forms describing the results well in quite wide regions $p \lesssim 0.25$ and $p^*-p \lesssim 0.25$ can be obtained by multiplying the corresponding expressions (30),(32) and (31),(33). The resulting curves are also shown in the figure. The initial linear reduction $M(p)/M(0) = 1 - B_0 p$, where the coefficient and its estimated error is $B_0 = 1.44 \pm 0.05$. At the percolation threshold the leading behavior is $M(p) = A_*(p^*-p)^{5/36}$ with $A_* = 0.137 \pm 0.002$.

In Ref. 12, the sublattice magnetization normalized by the number of magnetic sites, $M'(p) = M(p)/(1-p)$, which is equivalent to the quantum-mechanical factor M_{qm} for small p, was calculated using spin-wave theory with a T-matrix approximation. The initial linear weak-dilution form $M'(p)/M'(0) = 1 - B_0' p$, with $B_0' = 0.691 \pm 0.005$, was found in that approximation. The results obtained here for $M(p)$ correspond to a slightly smaller coefficient, $B_0' = 0.44 \pm 0.05$. Despite this difference in initial slope, the relative

agreement between the full sublattice magnetization shown in Fig. 18 and the corresponding spin-wave result is very good up to $p \approx 0.15$ (not shown here—see Fig. 10 of Ref. 41). For higher p, the spin-wave result falls significantly below the QMC result until very close to the percolation point, where the actual $M(p)$ approaches zero but the spin-wave result remains finite.[41] For $p \lesssim 0.35$, the results shown in Fig. 18 agree well with those presented previously by Kato *et al.*[17] Their extrapolations closer to the percolation threshold are not reliable, however, since they fitted a different, non-classical exponent to describe the $p \to p^*$ behavior. The estimated accuracy for the $M(p)$ curve obtained here is better than 2% over the whole range of dilutions (significantly better for $p \lesssim 0.1$).

VI. SPIN STIFFNESS

As discussed in Sec. II B, the spin stiffness ρ_s can be obtained in SSE simulations in terms of the winding number fluctuations, Eq. (14). At dilution fractions $p > p^*$ there are no clusters wrapping around the periodic $L \times L$ lattice for large L, and therefore the stiffness vanishes identically. Exactly at the percolation threshold the wrapping probability in a given direction is approximately 0.52,[16] and the stiffness can then be nonzero for finite L. It should vanish in the thermodynamic limit, however. For $p < p^*$ the wrapping probability approaches 1 as $L \to \infty$ and in view of the existence of antiferromagnetic long-range order the stiffness can then be expected to be nonzero.

For the classical diluted Heisenberg model the behavior of the stiffness (or helicity modulus) is known.[25] It scales in the same way as the conductivity of a random resistor network, with the conductivity exponent t of percolation.[42] According to recent simulations, the value of this exponent is $t = 1.310(1)$.[43] With the long-range order present in the per-
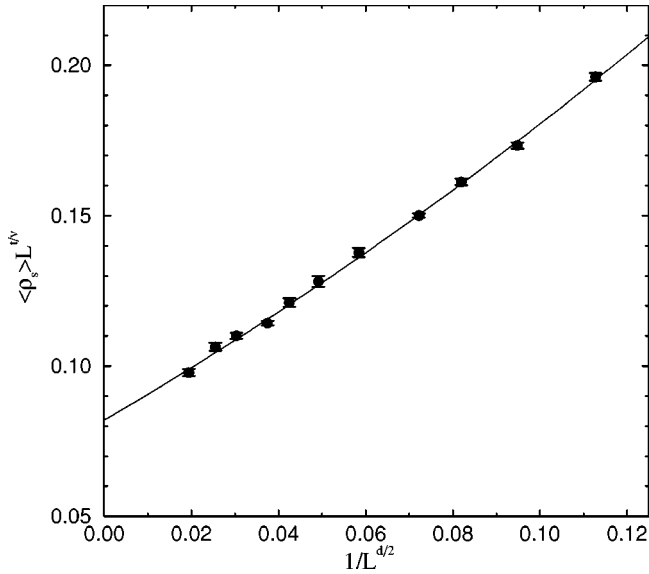
FIG. 19. Spin stiffness of site diluted $L \times L$ systems multiplied by $L^{t/\nu}$. The curve is a quadratic polynomial in $L^{-d/2}$.

FIG. 20. Infinite-size extrapolated spin stiffness vs dilution fraction (circles). The solid line is $\rho_s(p) = 0.1808 - 0.62p$. The dotted curve is the scaling form $\rho_s(p^*-p) \sim (p^*-p)^t$, and the dashed curve is a nonlinear σ-model result (Ref. 8).

colating clusters of the quantum Heisenberg model, as demonstrated in Sec. IV, one can expect that the stiffness should behave as in the classical model (in analogy with the "renormalized classical" behavior of the clean 2D Heisenberg model,[1] and in view of general symmetry arguments). Scaling with the conductivity exponent will therefore be tested here. It can be noted that the elastic moduli of a diluted classical elastic lattice also obey scaling with the conductivity exponent, if the force constants are isotropic.[44] With nonisotropic forces other scalings have been shown to be possible, and the critical dilution fraction above which the rigidity vanishes can in fact be below the percolation density.[45]

The elastic moduli of classical percolating lattices have been studied extensively using numerical methods.[45,46] The primary scaling technique used there will be employed here as well. If the analogy with the random resistor network holds, the disorder averaged stiffness at the percolation point should scale as $L^{-t/\nu}$,[46] where ν is the correlation length exponent of percolation, which is known exactly; $\nu = 4/3$.[15] Figure 19 shows the stiffness of the site-diluted Heisenberg model at the percolation density, multiplied by $L^{t/\nu}$, where $t/\nu = 0.9826$ was used.[43] The data extrapolate to a finite value as $L \to \infty$, and hence the results are indeed consistent with the conductivity scaling. The average stiffness shown here was calculated by including only nonzero values of the stiffness in a given lattice direction, and was averaged also over the two equivalent directions. The simulations included only the largest cluster in the system. The fraction of nonzero stiffnesses is approximately 0.52 for all L, in agreement with the known[16] wrapping probability of clusters in periodic systems.

Figure 20 shows the full dilution dependence of the stiffness extrapolated to infinite system size. The behavior is almost linear up to $p \approx 0.15$. The fitted linear form $\rho_s(p) = 0.1808 - 0.62p$ is shown in the figure, along with an analytical result containing terms up to p^2 obtained using a non-

linear σ model and percolation theory in Ref. 8. The σ-model approach gives a quantum critical point below the percolation point, and the initial falloff is also faster than what is seen in the QMC data. The QMC data close to the percolation point are not well described by the random resistor network exponent, although the results at the percolation point indicate that this should be the asymptotic form as $p \to p^*$. The critical region may be very small, however, making it difficult to observe in direct calculations for $p < p^*$.
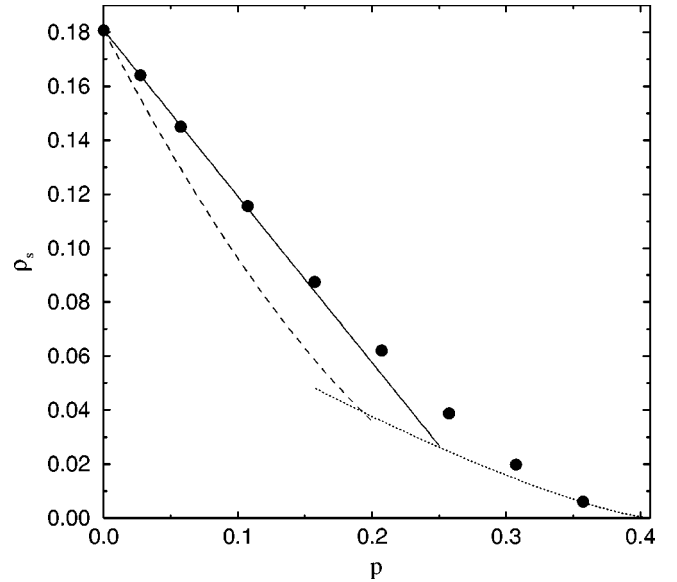
VII. SUMMARY AND DISCUSSION

This paper has presented a variety of quantum Monte Carlo results showing that the order-disorder transition in the diluted $S = 1/2$ Heisenberg model is solely driven by classical percolation. This is a consequence of the fractal clusters at the percolation point having long-range antiferromagnetic order. The presence of this long-range order was demonstrated by studying the largest cluster on $L \times L$ lattices, as well as clusters of fixed size N_c on the infinite 2D lattice. For the infinite-size extrapolated sublattice magnetization, the same nonzero value was obtained for both types of clusters. An accurate calculation of the sublattice magnetization M versus site dilution p was made possible by taking advantage of a factoring into classical and quantum-mechanical functions, which were evaluated separately. The classical factor is identical to the magnetization of a classical ferromagnet, and was calculated to high accuracy using lattice sizes L up to 4096. It contains the critical behavior of $M(p)$ close to the percolation point p^*. The quantum-mechanical factor is equivalent to the sublattice magnetization of the largest cluster on $L \times L$ lattices in the limit $L \to \infty$. It remains nonsingular as $p \to p^*$ and can be reliably extrapolated using relatively small system sizes (here using $L \leq 64$). Its infinite-size value grows

only by a factor 2 between $p=p^*$ and $p=0$. Approximate analytical forms describing the numerical $M(p)$ for all p were also constructed. The spin stiffness at the percolation point was shown to obey the same scaling as the conductivity of a random resistor network.

The conclusions reached in this paper differ from the nonuniversal quantum criticality scenario, which has been elucidated in several recent papers.[17,20,21] According to this scenario, the fractal clusters at the percolation point have power-law decaying spin-spin correlations, which implies that the scaling exponents differ from those of classical percolation. It was argued that the exponents depend on the spin S of the magnetic sites, so that classical percolation is recovered only for $S \to \infty$.[17] Several types of scaling analyses have been presented in support of this unusual behavior.[17,20,21] It can be noted, however, that only a very small number of system sizes were used. Temperature effects, although small,[19] may also have contributed to making the scaling appear better than it would be for real $T=0$ data.

The most serious problem with the finite-size scalings carried out in Refs. 17, 20, and 21 is that even if the percolating clusters are ordered, as they in fact are, the staggered structure factor cannot be expected to show the asymptotic classical scaling behavior for the range of system sizes used (as shown in Fig. 14). This is due to the strong size dependence of the sublattice magnetization of the clusters (in contrast to the classical case, in which the cluster magnetization takes its maximum value at $T=0$ for any system size). The classical scaling form is valid only for systems sufficiently large for the relative size corrections to be small, which is the case only for systems much larger than those that are currently accessible to quantum Monte Carlo simulation. This problem was circumvented here by focusing on the *cluster-size normalized* sublattice magnetization of the largest cluster of the lattice, which in combination with the known scaling of the cluster sizes completely determines the asymptotic behavior of the diluted system.

In Ref. 20 it was argued that the previous data[19] for the cluster magnetization for system sizes L up to 48 are also consistent with the quantum criticality scenario. On a log-log plot, the last few points were fitted to a straight line, and the same exponent as that previously extracted from the staggered structure factor was obtained. The use of only a few system sizes in such a scaling is dangerous, however. It neglects the slow curvature that is evident in the data.[20] With one more system size now available ($L=64$), as well as increased precision for smaller L, the failure of the quantum critical scaling can be demonstrated even more clearly. Figure 21 shows a log-log plot of the cluster magnetization along with a line with a slope 0.52, which was previously argued to describe the data.[20] The $L=64$ point does not fall on the line, and also the smaller systems show deviations beyond the statistical errors. A slow upward curvature as $L \to \infty$ is evident. With no indication of a vanishing cluster magnetization on the linear scale in Fig. 10, the log-log plot is clearly not suitable for analyzing the data.

In earlier Monte Carlo studies of disordered Heisenberg models[6,10] it was concluded that the antiferromagnetic order vanishes in a quantum phase transition before the classical
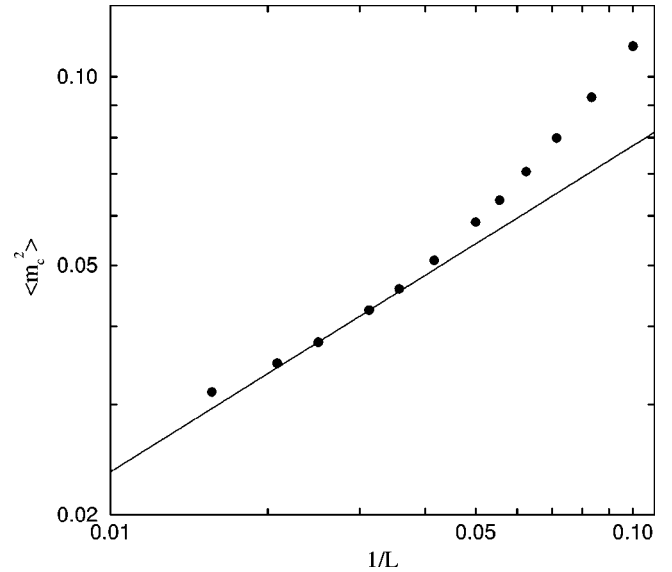
FIG. 21. The cluster magnetization vs inverse system size on a log-log scale. The statistical errors are smaller than the circles. The line has a slope 0.52, which was previously argued[20] to be the quantum critical scaling exponent.

percolation threshold. With the current results for much larger lattices at hand, it is clear that state-of-the-art simulations at earlier times were not able to reach sufficiently large system sizes for observing the true asymptotic behavior. The essentially linear extrapolations used to extract the critical point were therefore misleading. Similar work on the disordered half-filled Hubbard model on small lattices also have indicated that quantum fluctuations destroy the order before the percolation point.[47] In light of the behavior of the Heisenberg model, it would be interesting to repeat these calculations using larger lattice sizes. For the Hubbard model it is currently not possible to reach system sizes as large as for the Heisenberg model, however.

Experiments on quasi-2D cuprate antiferromagnets doped with nonmagnetic impurities have in the past been able to reach only dilution fractions $\lesssim 20\%$.[11] The doping dependence in this region is in reasonable agreement with calculations.[8] Recently, improved sample preparation techniques, involving simultaneous doping with Zn and Mg, have enabled studies of La_2CuO_4 all the way to the percolation threshold.[13] Neutron-scattering measurements of the temperature dependence of the correlation length and the sublattice magnetization indicate that the order persists until $p \approx p^*$,[13] in accord with the behavior of the Heisenberg model discussed here. It can be noted that both the sublattice magnetization and the spin stiffness extracted in the experiments[13] agree reasonably well with the curves extracted here (Figs. 18 and 20) at weak dilution but fall significantly faster to zero as the percolation threshold is approached. This is an indication of additional quantum fluctuation mechanisms weakening (but not destroying) the long-range order, with likely candidates being frustrating next-nearest-neighbor interactions and four-spin ring exchange.[48] The effects of these interactions are likely more pronounced in the diluted systems. Random lattice distor-

tions causing fluctuations in the nearest-neighbor couplings could also play a role.

In a system exhibiting a quantum phase transition as a function of some model parameter, e.g., the Heisenberg bilayer,[49] certain types of dilution can drive an order-disorder transition before the classical percolation threshold. If the dilution leads to magnetic moment formation the phase transition is destroyed, however, since the moments interact and order even in the gapped phase.[28] In the bilayer, dilution of interlayer dimers (two adjacent spins on opposite layers) does not lead to moment formation, and a quantum phase transition can occur before the percolation threshold (as a function of the dilution fraction or the interlayer coupling). A multicritical point, where the percolating cluster is quantum critical, has recently been demonstrated in this system.[50]

Quantum disordered ground states have also been found in Heisenberg antiferromagnets on nonrandom fractal lattices, such as the Sierpiński gasket.[51]

[1] S. Chakravarty, B. I. Halperin, and D. R. Nelson, Phys. Rev. Lett. **60**, 1057 (1988); Phys. Rev. B **39**, 2344 (1989).

[2] S. Sachdev, *Quantum Phase Transitions* (Cambridge University Press, Cambridge, 1999).

[3] N. Read and S. Sachdev, Phys. Rev. Lett. **62**, 1694 (1989); **66**, 1773 (1991).

[4] R. R. P. Singh, M. P. Gelfand, and D. A. Huse, Phys. Rev. Lett. **61**, 2484 (1988).

[5] E. Manousakis, Phys. Rev. B **45**, 7570 (1992).

[6] J. Behre and S. Miyashita, J. Phys. A **25**, 4745 (1992); S. Miyashita, J. Behre, and S. Yamamoto, in *Quantum Monte Carlo Methods in Condensed Matter Physics*, edited by M. Suzuki (World Scientific, Singapore, 1994).

[7] C. Yasuda and A. Oguchi, J. Phys. Soc. Jpn. **66**, 2836 (1997); *ibid.* **68**, 2773 (1999).

[8] Y.-C. Chen and A. H. Castro Neto, Phys. Rev. B **61**, R3772 (2000).

[9] C. C. Wan, A. B. Harris, and J. Adler, J. Appl. Phys. **69**, 5191 (1991).

[10] A. W. Sandvik and M. Vekić, Phys. Rev. Lett. **74**, 1226 (1995).

[11] S.-W. Cheong *et al.*, Phys. Rev. B **44**, 9739 (1991); S. T. Ting *et al.*, *ibid.* **46**, 11 772 (1992); M. Corti *et al.*, *ibid.* **52**, 4226 (1995); P. Carretta, A. Rigamonti, and R. Sala, *ibid.* **55**, 3734 (1997).

[12] A. L. Chernyshev, Y. C. Chen, and A. H. Castro Neto, Phys. Rev. Lett. **87**, 067209 (2001).

[13] O. P. Vajk, P. K. Mang, M. Greven, P. M. Gehring, and J. W. Lynn, Science **295**, 1691 (2002).

[14] N. Bulut, D. Hone, D. J. Scalapino, and E. Y. Loh, Phys. Rev. Lett. **62**, 2192 (1989); T.-K. Ng, Phys. Rev. B **54**, 11 921 (1996); A. W. Sandvik, E. Dagotto, and D. J. Scalapino, *ibid.* **56**, 11 701 (1997); V. N. Kotov, J. Oitmaa, and O. Sushkov, *ibid.* **58**, 8495 (1998).

[15] D. Stauffer and A. Aharony, *Introduction to Percolation Theory* (Taylor and Francis, London, 1991).

[16] M. E. J. Newman and R. M. Ziff, Phys. Rev. Lett. **85**, 4104 (2000).

[17] K. Kato *et al.*, Phys. Rev. Lett. **84**, 4204 (2000); S. Todo *et al.*, Int. J. Mod. Phys. C **10**, 1399 (1999).

[18] M. Suzuki, Prog. Theor. Phys. **51**, 1992 (1974).

[19] A. W. Sandvik, Phys. Rev. Lett. **86**, 3209 (2001).

[20] S. Todo, H. Takayama, and N. Kawashima, Phys. Rev. Lett. **86**, 3210 (2001).

[21] C. Yasuda *et al.*, Phys. Rev. B **63**, 140415(R) (2001).

[22] A. W. Sandvik and J. Kurkijärvi, Phys. Rev. B **43**, 5950 (1991); A. W. Sandvik, J. Phys. A **25**, 3667 (1992).

[23] A. W. Sandvik, Phys. Rev. B **56**, 11 678 (1997).

[24] A. W. Sandvik, Phys. Rev. B **59**, R14 157 (1999).

[25] A. B. Harris and T. C. Lubensky, Phys. Rev. B **35**, 6964 (1987).

[26] P. Henelius and A. W. Sandvik, Phys. Rev. B **62**, 1102 (2000).

[27] A. W. Sandvik, Phys. Rev. Lett. **83**, 3069 (1999); P. V. Shevchenko, A. W. Sandvik, and O. P. Sushkov, Phys. Rev. B **61**, 3475 (2000); A. W. Sandvik and R. R. P. Singh, Phys. Rev. Lett. **86**, 528 (2001).

[28] S. Wessel, B. Normand, M. Sigrist, and S. Haas, Phys. Rev. Lett. **86**, 1086 (2001).

[29] R. T. Clay, S. Mazumdar, and D. K. Campbell, Phys. Rev. Lett. **86**, 4084 (2001).

[30] A. Dorneich and M. Troyer, Phys. Rev. E **64**, 066701 (2001).

[31] In cases where memory size is a limiting factor, more efficient packing of the data can further reduce the requirements. The size of the linked list representing the configuration in the operator-loop update is also strictly smaller than M, typically by about 20%, since no [0,0] elements need to be stored.

[32] J. D. Reger and A. P. Young, Phys. Rev. B **37**, 5978 (1988).

[33] T. Einarsson and H. J. Schulz, Phys. Rev. B **51**, 6151 (1995).

[34] A. Paramekanti, N. Trivedi, and M. Randeria, Phys. Rev. B **57**, 11 639 (1998).

[35] J. Oitmaa and O. Sushkov, Phys. Rev. Lett. **87**, 167206 (2002).

[36] P. Henelius, S. M. Girvin, and A. W. Sandvik, Phys. Rev. B **57**, 13 382 (1998).

[37] B. Efron and G. Gong, Am. Stat. **37**, 36 (1983).

[38] D. A. Huse, Phys. Rev. B **37**, 2380 (1988).

[39] J. Marro, Phys. Lett. **59A**, 180 (1976); D. S. Gaunt and H. Ruskin, J. Phys. A **11**, 1369 (1978).

[40] The staggered structure factor data presented in Ref. 17 were in fact based on the largest cluster, S. Todo (private communication).

[41] A. L. Chernyshev, Y. C. Chen, and A. H. Castro Neto, Phys. Rev. B **65**, 104407 (2002).

[42] A. B. Harris and R. Fisch, Phys. Rev. Lett. **38**, 796 (1977).

[43] P. Grassberger, Physica A **262**, 251 (1999).

[44] P. G. de Gennes, J. Phys. (France) **37**, L-1 (1976).

[45] S. Feng and P. N. Sen, Phys. Rev. Lett. **52**, 216 (1984); Y. Kantor and I. Webman, *ibid.* **52**, 1891 (1984).

[46] C. J. Lobb and D. J. Frank, J. Phys. C **12**, L827 (1979); Phys. Rev. B **30**, 4090 (1984); S. Feng, P. N. Sen, B. I. Halperin, and C. J. Lobb, *ibid.* **30**, 5386 (1984).

[47] M. Ulmke and R. T. Scalettar, Phys. Rev. B **55**, 4149 (1997).

[48] R. Coldea *et al.*, Phys. Rev. Lett. **86**, 5377 (2001).

[49] K. Hida, J. Phys. Soc. Jpn. **59**, 2230 (1990); A. J. Millis and H. Monien, Phys. Rev. B **50**, 16 606 (1994); A. W. Sandvik and D. J. Scalapino, Phys. Rev. Lett. **72**, 2777 (1994).

[50] A. W. Sandvik, cond-mat/0206355 (unpublished).

[51] A. Voigt, J. Richter, and P. Tomczak, Physica A **299**, 107 (2001).